Cryogenic Germanium Power Diode Circuit Simulator Model Including Temperature Dependent Effects

S.G. Pytel, A.S. Hoenshel, L. Lu, E. Santi, J.L. Hudgins*, P.R. Palmer**

Department of Electrical Engineering
University of South Carolina
301 South Main Street
Columbia, South Carolina 29208
Pyteljr@engr.sc.edu

*Department of Electrical Engineering
University of Nebraska
209N WSEC
Lincoln, Nebraska 68588-0511

** Department of Engineering
University of Cambridge
Trumpington Street
Cambridge CB2 1PZ, UK

Abstract

Cryogenic testing and physics-based device modeling of a germanium (Ge) power diode for power electronic applications has been conducted. Static and inductive load testing of a 10 A, 250 V Ge diode has been performed with temperatures ranging from ambient (~ 300 K) to liquid nitrogen (77 K). The device was modeled using the Fourier-series-based solution approach for PvN diodes. The Fourier solution was used in the development of a temperature-dependent physics-based model that can be run using simulation software packages such as Virtual Test Bed (VTB) or PSPICE™. This model has proven to be extremely accurate when applied to silicon based power diodes and similar results have been obtained for the cryogenic Ge diode. Formulas for the temperature dependency of Ge physical parameters, such as mobilities, intrinsic carrier concentration and ionized impurity concentration, are extracted from published data and implemented in the model. Since very limited data is available for the temperature dependence of carrier recombination lifetime, its temperature dependence is extracted from experimental data. Interest in Ge power devices and reliable circuit simulator models is driven by low temperature applications such as deep space exploration, medical diagnostics, and superconductive energy storage.

List of Symbols

D	Ambipolar diffusion coefficient (cm^2/s)
E_C	Conduction band energy (eV)
E_D	Donor energy level within the gap (eV)
E_F	Fermi energy level (eV)
E_G	Bandgap energy (eV)
E_V	Valence band energy (eV)
g_D	Donor degeneracy factor
k	Boltzmann's constant (eV/K)
m_o	Electron rest-mass (kg)
m_e^*	Electron density of states effective-mass (kg)
m_p^*	Hole density of states effective-mass (kg)
μ_n	Electron mobility (cm^2/Vs)
μ_p	Hole mobility (cm^2/Vs)
n	Electron concentration (cm^{-3})
n_i	Intrinsic carrier concentration (cm^{-3})
N_A	Acceptor impurity doping concentration (cm^{-3})
N_C	Effective density of states (cm^{-3})
N_D	Donor impurity doping concentration (cm^{-3})
N_A^-	Ionized acceptor concentration (cm^{-3})
N_D^+	Ionized donor concentration (cm^{-3})
N_t	Recombination center (trap) density (cm^{-3})
$p(x,t)$	Excess carrier concentration (cm^{-3})
p	Hole concentration (cm^{-3})
t	Time (s)
τ	High-level carrier lifetime (s)
τ_0	High-level lifetime at 300 K (s)
T	Absolute temperature (K)
x	Distance along drift/base region (cm)
x_1	Carrier storage region boundary (cm)
x_2	Carrier storage region boundary (cm)

I. INTRODUCTION

Cryogenic operation of electronic devices has become increasingly important. The demand for cryogenic electronic devices stems from the inability to perform extended deep space exploration due to the inefficiencies associated with standard operating electronic devices, which typically operate in a range of temperatures from -55°C to +125°C [1]. Standard electronic devices operating in space normally incorporate heaters to ensure that their operating temperature does not fall below the minimum operating temperature [2]. It is highly desirable to employ devices that can operate at cryogenic temperatures and eliminate the heaters. There are also several commercial applications where cryogenic devices would be advantageous: medical diagnostics (MRI) [3], power transmission and distribution systems that use superconductors [4-5], superconducting inductors [6-9], superconducting magnets [10], and magnetic confinement systems [11].

Germanium (Ge) devices are well suited for cryogenic operation due to their low dopant ionization energy. This allows Ge devices to operate at extremely low temperatures. The freeze-out temperature for dopants in silicon (Si) is approximately 40 K compared to 20 K in Ge devices [12]. Other advantages of Ge over Si are higher electron and hole mobilities, which result in faster switching speeds, and lower bandgap energy, which results in a lower forward voltage drop [13].

In Section II the Fourier-based electro-thermal diode model is briefly reviewed. In Section III temperature dependencies of Ge material properties such as mobilities,

intrinsic carrier concentration and ionized impurity concentration are extracted from published data. These temperature dependencies are needed for the implementation of the Ge diode model. In Section IV experimental results for a 250 V, 10 A Ge power diode are reported. In Section V simulation and experimental results for the diode reverse recovery are compared at various temperatures from 77 K to 300 K.

II. ELECTRO-THERMAL PHYSICS-BASED MODEL

The basis for the temperature-dependent physics-based model comes from a Fourier solution to the ambipolar diffusion equation (1) [14], which describes the dynamics of the carrier distribution in the drift region. This simplified ambipolar diffusion equation assumes a one-dimensional carrier distribution in the drift region and high level injection [15].

$$D\frac{\partial^2 p(x,t)}{\partial x^2} = \frac{p(x,t)}{\tau} + \frac{\partial p(x,t)}{\partial t} \qquad (1)$$

The carrier distribution can be expanded in a Fourier series as follows:

$$p(x,t) = p_o(t) + \sum_{k=1}^{\infty} p_k(t)\cos\left[\frac{k\pi(x-x_1)}{x_2 - x_1}\right] \qquad (2)$$

Substituting this expression for the carrier distribution into the ambipolar equation (1) transforms the 2nd order partial differential equation into an infinite series of 1st order linear differential equations. These equations may be solved in a circuit-based simulator by transforming each 1st order linear differential equation into an equivalent R-C network [15].

III. MATERIAL PARAMETERS AT LOW TEMPERATURES

A. Carrier Mobilities

Very little data is available for material parameters for Ge, particularly at low temperatures (below 100 K). Some hole and electron mobility curves have been presented in [16]. In particular, we are interested in the data associated with carrier mobilities for low impurity doping levels. Data extracted from [16], for doping levels of about 10^{13} cm^{-3}, have been used to calculate a least squares fit to a power regression curve for hole mobility and is given by (3).

$$\mu_p = 1.042\times10^7 T^{-1.39} \qquad (3)$$

The equation (3) is fitted to data for temperatures between 5 and 300 K and thus can be considered valid over that range. However, (4) is often used to describe the temperature dependence of the hole mobility in Ge for temperatures from 100 to 300 K [17].

$$\mu_p = 1.05\times10^9 T^{-2.33} \qquad (4)$$

A comparison of (3) and (4) is illustrated in Figure 1. The data used from [16] are included to show the fit.

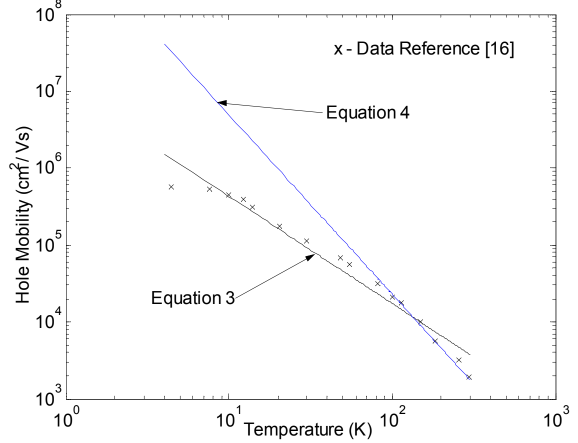

Figure 1: Hole mobility as a function of temperature from 4.2 to 300 K.

Note that (4) fits the data well for temperatures above 100 K, but diverges rapidly from the reported values below 100 K. For Ge devices operated cryogenically, we recommend using (3) to describe the temperature dependence of the hole mobility. Above 100 K, (4) fits the data better and should be used. However, (3) will give a reasonable value of hole mobility up to 300 K if only one relationship is to be used for modeling.

The electron mobility as a function of temperature was calculated using a least squares fit to a power regression curve from data in [16], and is given by (5). It is valid over the temperature range from 4.2 to 300 K.

$$\mu_n = 1.892\times10^7 T^{-1.42} \qquad (5)$$

The relationship given in (6) is often used to describe the temperature dependence of the electron mobility [17]. It was described as being valid only from 77 to 300 K.

$$\mu_n = 4.9\times10^7 T^{-1.655} \qquad (6)$$

Figure 2 compares (5) and (6) along with the data used to create (5). Note that (6) overestimates the mobility value below 77 K and underestimates the value above 100 K. Based on the spread of values of electron mobility (from around 3900 to 5700 cm^2/Vs) cited at room temperature, (5) gives a value at the high end of the range while (6) gives a value at the low end. Because (5) is a least squares fit, we recommend using this relationship for the temperature dependence of electron mobility for all temperatures below 300 K, and in particular for cryogenic operation of devices.

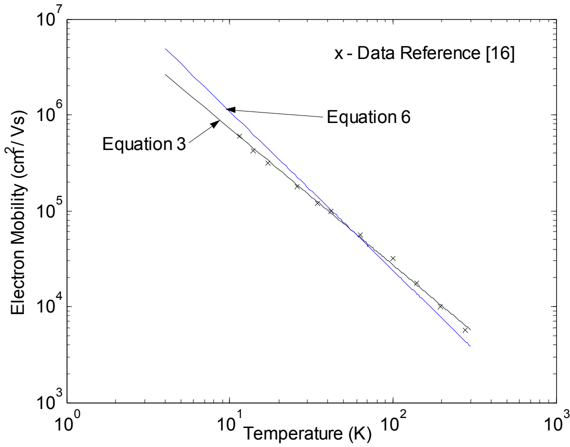

Figure 2: Electron mobility as a function of temperature from 4.2 to 300 K.

B. *Energy Bandgap and Intrinsic Carrier Concentration*

The temperature dependence of the energy bandgap is given in (7) from [18]. From (7), the intrinsic carrier concentration as a function of temperature (8), including bandgap changes with temperature, can be derived similarly to the expression given in [18].

$$E_G = 0.742 - 4.8\times10^{-4}\left(\frac{T^2}{T+235}\right) \qquad (7)$$

$$n_i = 1.76\times10^{16}T^{1.5}e^{\left(\frac{-E_G}{2kT}\right)} \qquad (8)$$

A graph of (8) incorporating (7) is shown in Figure 3. The values shown from 6 to 300 K are normalized with respect to the intrinsic carrier concentration value at 300 K. At temperatures below 100 K, the intrinsic carrier concentration is many orders of magnitude lower then at room temperature. This effect on n_i must be taken into account to accurately describe the low-temperature behavior of any devices operating cryogenically.

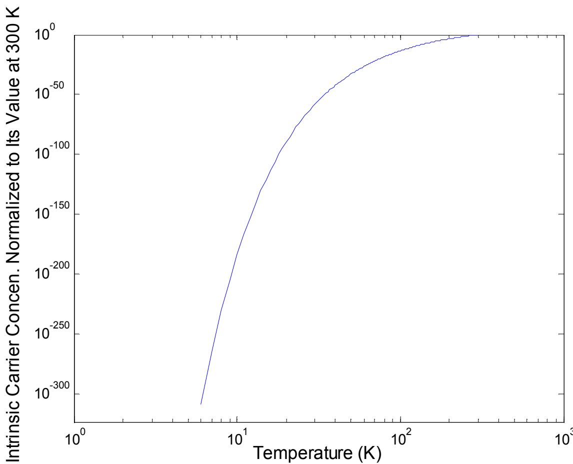

Figure 3: The intrinsic carrier concentration, normalized to its value at 300 K, over the temperatures from 6 to 300 K.

C. *Ionized Impurity Concentration*

Almost all of the impurity atoms are ionized at temperatures above 0 °C, but below this temperature the incomplete ionization should be accounted for in the donor concentration. A formula for the ionized donor impurity concentration has been previously derived [19]. The ionized donor concentration is given by

$$n = N_D^+ = \frac{N_C}{2g_D}e^{-(E_C-E_D)/kT}\left[\left(1+\frac{4N_D}{(N_C/g_D)e^{-(E_C-E_D)/kT}}\right)^{1/2}-1\right] \qquad (9)$$

where

$$N_C = n_i e^{(E_c-E_i)/kT} = n_i\left(\frac{m_n^*}{m_p^*}\right)^{3/4} e^{E_G/2kT} \qquad (10)$$

It is assumed that the ratio of the density-of-states effective masses in (10) is constant with respect to temperature. The donor degeneracy factor, g_D, is usually assumed to be equal to 2 to account for electron spin, with E_D as the donor energy level within the gap. The effect of temperature on the ionization of arsenic impurity atoms in Ge, at a concentration of about 9 x 10^{13} cm^{-3}, is described by (9) and (10) in Figure 4. Note that 90% of the donor atoms are ionized even at 20 K.

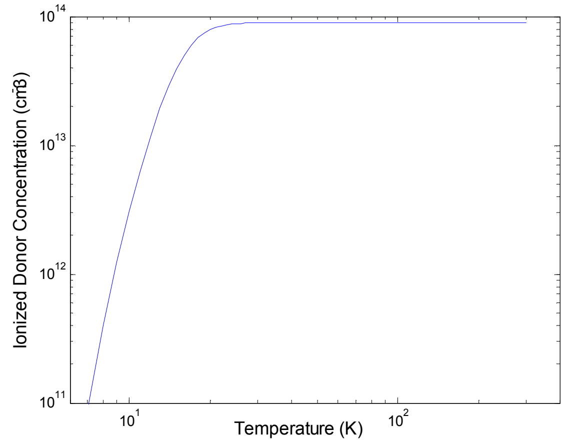

Figure 4: Ionized donor concentration as a function of temperature.

The ionized donor impurity concentration drops to about 10^{11} cm^{-3} at 7K. It is clear from this analysis that Ge, with a background impurity concentration of 10^{13} cm^{-3} or greater, will operate quite effectively down to at least 12 K.

D. *Carrier Recombination Lifetime*

Very limited data [16] was found in the literature on the temperature dependence of minority carrier recombination (holes or electrons) in Ge. Therefore, the recombination lifetime was extracted from our own experimental data. An inductive load test was performed at various temperatures and the recombination lifetime extracted at each temperature according to the parameter extraction procedure described in [15]

A least squares power regression relationship was performed on the data obtained. It was found that for the device under study the temperature dependence is actually linear. A more extensive characterization of lifetime using more data points and going to lower temperatures is left as future work. The empirical behavior of lifetime (11) is plotted in Figure 5, along with the data.

$$\tau = \tau_0\left(\frac{T}{300}\right) \qquad (11)$$

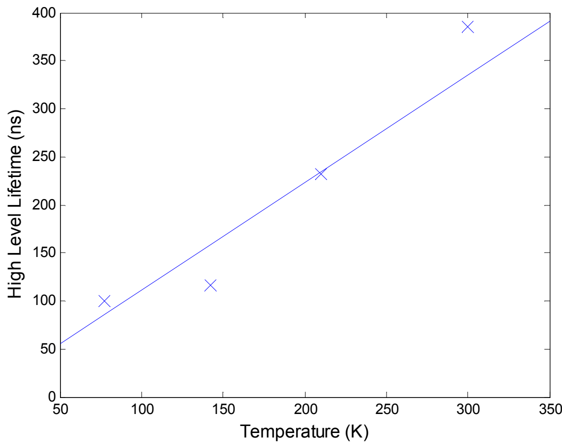

Figure 5: High-level carrier recombination lifetime as a function of temperature from experimental data.

IV. EXPERIMENTAL RESULTS

A. Static Testing

Static current and voltage measurements were performed between ambient temperature (300 K) and 77 K on a 250 V, 10 A Ge power diode. The static tests were performed using a Tektronix 371A high power curve tracer. The forward voltage drop characteristics of this diode at 300 K and 77 K are shown in Figures 6 and 7 respectively. Notice the Ge diode exhibits a much lower on-state voltage than typical Si diodes at either 300 K or 77 K.

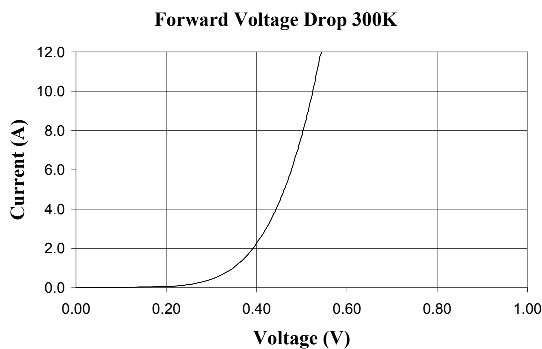

Figure 6: Germanium power diode forward voltage drop at 300 K.

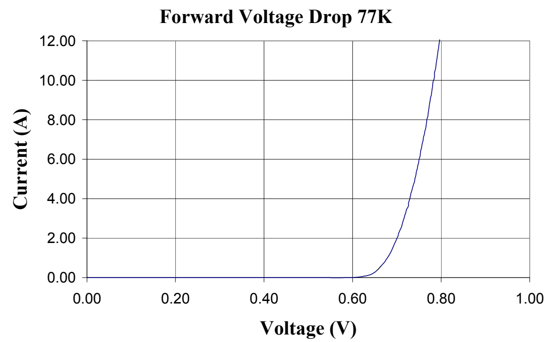

Figure 7: Germanium power diode forward voltage drop at 77 K.

The reverse breakdown voltage of the Ge diode is shown in Figures 8 and 9 for 300 K and 77 K respectively. The Ge diode is quite leaky at ambient temperature and this can be seen by the soft reverse breakdown curve in Figure 8 at 300 K. At 77 K the leakage current of the diode is reduced and reverse breakdown voltage of approximately 350V is obtained.

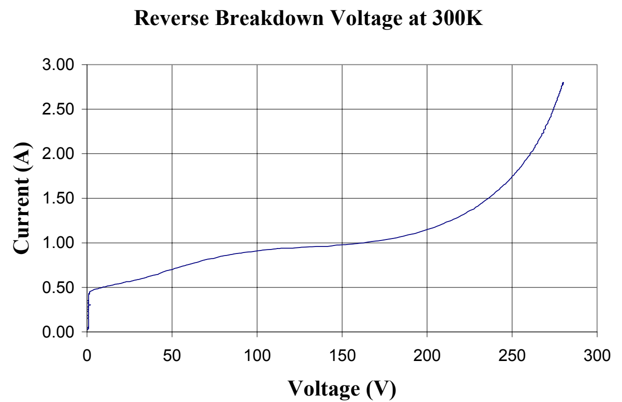

Figure 8: Germanium diode reverse characteristics at 300 K.

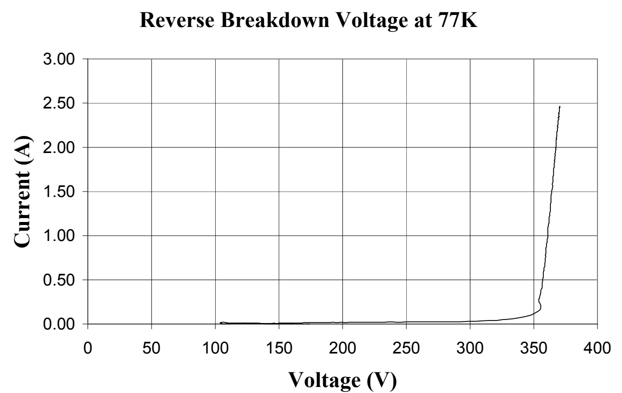

Figure 9: Germanium diode reverse characteristics at 77 K.

B. Dynamic Load Testing

Dynamic inductive load tests were performed with the circuit shown in Figure 10 for temperatures below 300 K. The Ge diode was tested between ambient temperature (300 K) and 77 K. At 300 K the RC snubber branch was omitted, but below this temperature the RC snubber was used to minimize parasitic ringing in the circuit.

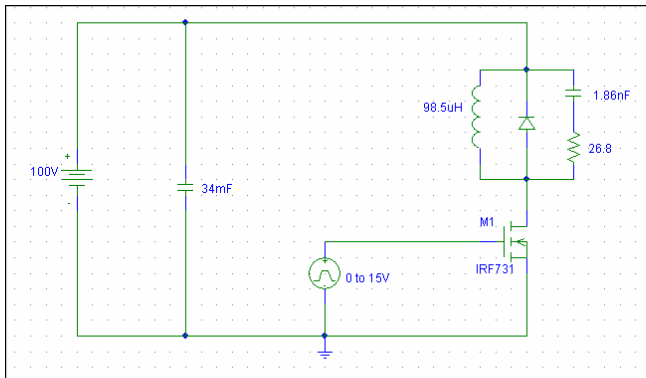

Figure 10: Experimental circuit. Note the RC snubber was not used at 300 K.

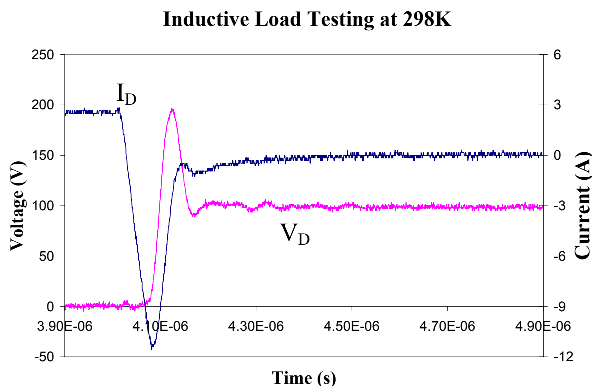

Figure 11: Dynamic load testing of germanium diode at 298 K.

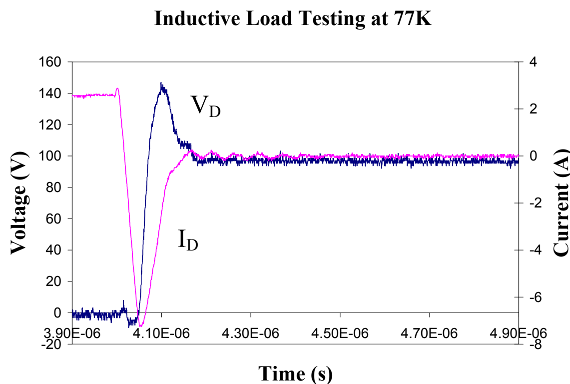

Figure 12: Dynamic load testing of germanium diode at 77 K.

The experiment used an environmental chamber to control the cool-down and heat-up of the device. The temperature was measured using a Lakeshore DT670SD diode sensor mounted to the outside of the Ge diode package. The RC snubber circuit used for temperatures below 300 K was placed inside the temperature chamber, and it was connected directly across the diode. The current sensor was connected outside of the temperature chamber and resulted in the measured current being the combination of the RC snubber current and diode current. The true diode current was reconstructed based on the measured current and the measured diode voltage.

The inductive switching waveforms at ambient temperature (300 K) and 77 K are shown in Figure 11 and 12 respectively. The steady state current was limited to 2.5 A due to the limited current capacity of the diode's bonding wires. With an input voltage of 100 V, the maximum reverse recovery current at room temperature is -11.4 A compared to -7.2 A at 77 K. As expected, the reverse recovery of the diode improves with lowering temperature [19].

V. SIMULATION RESULTS

A. Modifications to Fourier-Based-Solution Diode Model for Ge Material

The Fourier-based-solution model previously compiled for Si diodes [15] was reformulated for the Ge diode operating at cryogenic temperatures. Changes to the model were made based on the equations listed in Section III above. The diode physical parameters were provided by the manufacturer and used in the model as well. This ensures the model represents the actual physical structure of the Ge diode.

B. Reverse Recovery Current Dependence on High Level Lifetime

In the Fourier based solution model the diode reverse recovery current is a strong function of the minority carrier recombination lifetime. Figure 13 shows the Fourier based model dependence on high level lifetime for 50 ns, 75 ns, 100 ns, 125 ns, and 150 ns compared to the experimental data at 77 K. As carrier recombination lifetime increases the reverse recovery time and peak current magnitude increase due to the longer time before recombination of the carriers in the drift region. As can be seen from this figure, a value of τ_{HL} = 100ns gives a very good fit to the experimental data.

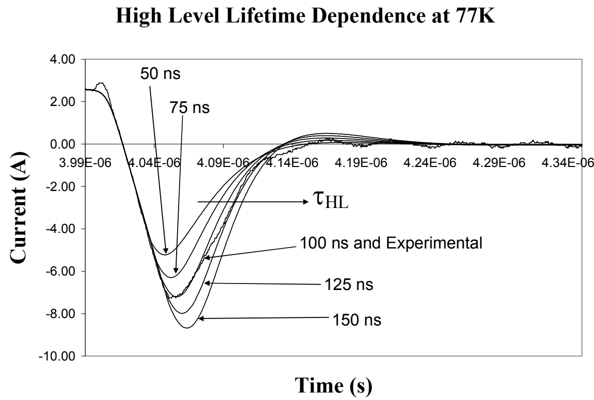

Figure 13: Simulated reverse recovery current at 77 K for different values of high level lifetime.

C. Comparison of Simulation and Experimental Results

Experiments were performed at room temperature (≈ 300 K), 210 K, 142 K, and 77 K. The results are shown in Figures 14, 15, 16, and 17 respectively. The actual extracted values of lifetime were used in the model rather than the least squares fit given by equation (11).

The reverse recovery currents match extremely well for all temperatures between 300 K and 77 K. The experimental diode voltages match fairly well with the simulation providing slightly more overshoot than the experiment. This is most likely due to guard rings that were not considered in the simulation. The added area of the guard rings should increase the diode capacitance thereby reducing the voltage overshoot predicted by the model. The addition of guard rings to the Fourier based solution model will be left for future work. The similarity between the experimental and simulated results shows the robustness of the model over changes in temperature.

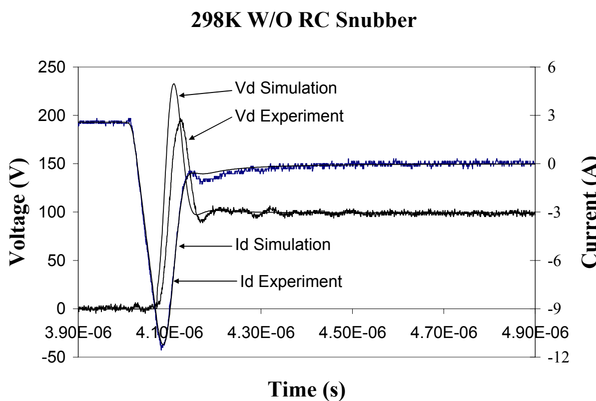

Figure 14: Comparison between simulation and experimental results for V_D and I_D at ambient temperature. The experimental setup does not include the RC snubber.

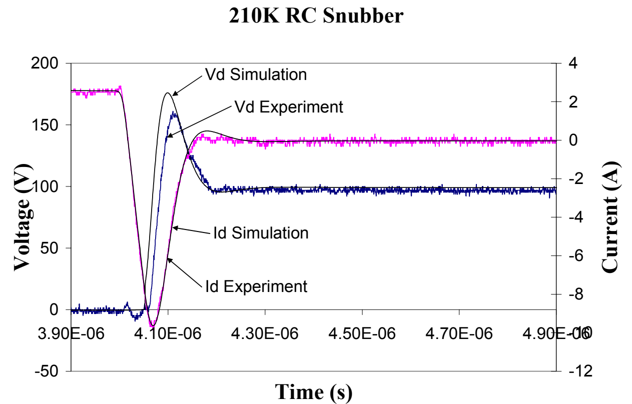

Figure 15: Comparison between simulation and experimental results for V_D and I_D at 210K. The experimental setup includes the RC snubber.

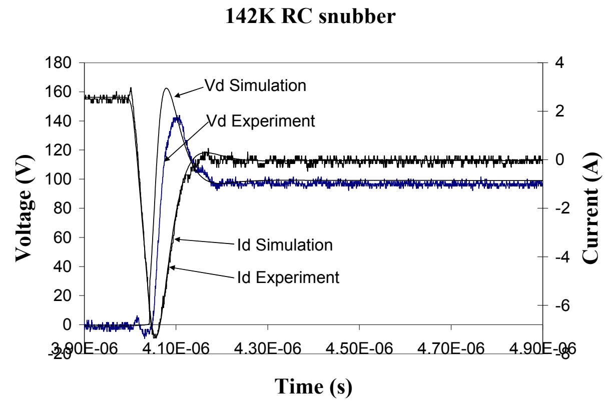

Figure 16: Comparison between simulation and experimental results for V_D and I_D at 142K. The experimental setup includes the RC snubber.

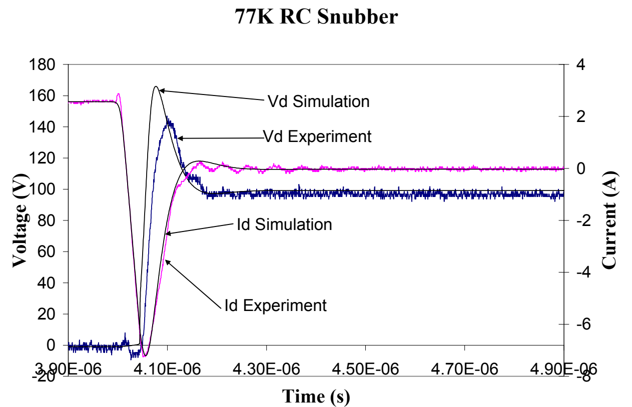

Figure 17: Comparison between simulation and experimental results for V_D and I_D at 77K. The experimental setup includes the RC snubber.

VI. Conclusion

There is a large need for cryogenic power electronic devices for applications ranging from space exploration to magnetic resonance imaging and superconductor systems. Germanium provides an excellent solution to the problems associated with Si devices at cryogenic temperatures. Therefore, it is highly desirable to be able to accurately and reliably predict the operation of these devices at cryogenic temperatures. A physics-based model using the Fourier solution to the ambipolar diffusion equation has been implemented into software platforms such as PSPICE^{TM} and has yielded accurate temperature dependent results for a cryogenic Ge diode over a wide temperature range. Additional work is needed to develop a temperature dependent equation that accurately determines the carrier recombination lifetime over temperature for Ge.

ACKNOWLEDGEMENT

This work was supported by the U.S. Office of Naval Research under Grants N00014-02-1-0623 and N00014-03-1-0434. The Ge diodes were provided by GPD Optoelectronics (Salem, New Hampshire), with support from the NASA Glenn Research Center, Low Temperature Electronics Program.

REFERENCES

[1] M. Newell, "Electronics for extremely cold environments: enabling new space missions," NASA Electronic Parts and Packaging (NEPP) '02 Workshop, Houston, Texas, 30 April-2 May 2002

[2] Ward, Dawson, Zhu, Kirschman, O. Mueller, Patterson, Dickman, and Hammoud; "Ge Semiconductor Devices for Cryogenic Power Electronics – III"; 15th *IEEE Int. Symposium on Power Semiconductor Devices and ICs*, pp 321–324, April 2003

[3] O. M. Mueller and E. K. Mueller, "Cryogenic power inverters for magnetic resonance (MRI) systems," *Proc. – 1999 Cryogenic Engineering Conference (CEC)*, Montreal, Quebec, Canada, 12-15 July 1999; *Advances in Cryogenic Engineering*, vol. 45B, pp. 1603-1612, 2000

[4] O. M. Mueller and E. K. Mueller, "Cryogenic power/energy distribution system," *Advances in Cryogenic Engineering*, vol. 45, pp. 1755-1762, 2000.

[5] O. M. Mueller and E. K. Mueller, "Efficient two-level cryogenic power distribution system," *Advances in Cryogenic Engineering*, vol. 47, pp. 1719-1725, 2002.

[6] J. F. Kärner, H. W. Lorenzen, F. Rosenbauer, J. Schaller and R. M. Schöttler, "A protection system for small high power SMES with power semiconductors working at cryogenic temperature," *IEEE Tr. on Applied Superconductivity*, vol. 5, no. 2, pp. 266-269, June 1995

[7] E. Perel et al., "Converter operating at liquid nitrogen temperatures for HT-SMES," *Proc. – 4th European Workshop on Low Temperature Electronics*, Noordwijk, Netherlands, 21-23 June 2000, pp. 163 (ESA Publication WPP-171)

[8] F. Rosenbauer and M. Harke, "Simulation and design of a protection system for SMES," *Proc. – 1997 Cryogenic Engineering Conference*, Portland, Oregon, August 1997; *Advances in Cryogenic Engineering*, vol. 44, Part B, pp. 1151-1158, 1998

[9] T. Ise and Y. Murakami, "Control of a superconducting coil by a MOSFET power converter operating at near liquid nitrogen temperature," *IEEE Trans. on Magnetics*, vol. 27, no. 2, pp. 2020-2023, March 1991

[10] O. A. Shevchenko, H. J. G. Krooshoop, M. A. Fedorovsky and H. H. J. ten Kate, "Cold semiconducting converter, a compatibility device for a superconducting magnet," *Proc. – 1995 Cryogenic Engineering Conference*; *Advances in Cryogenic Engineering*, vol. 41, pp.1873-1880, 1996

[11] T. Matsukawa, K. Shimada, M. Shioyama, T. Takaku, S. Tsuji-Iio and R. Shimada, "Novel application of power-MOSFET for energy electronics," *Extended Abstracts – 1st International Workshop on Ultra-Low-Loss Power Device Technology*, Nara, Japan, 31 May–2 June 2000, pp. 215-216 (FED-171)

[12] Ward, Dawson, Zhu, Kirschman, O. Mueller, Hennessy, E. Mueller, Patterson, Dickman, and Hammoud; "Power diodes for cryogenic operation"; *2003 IEEE 34th Annual Power Electronic Specialists Conference;* pp. 1891-1896, 15-19 June 2003

[13] Hudgins; "Wide and Narrow Bandgap Semiconductors for Power Electronics: A New Valuation"; *IEEE Journal of Electronic Materials*; V32, N6, pp. 471 – 477, 2003.

[14] Leturcq, Berraies, Debrie, Gillet, Kallala, and Massol, "Bipolar semiconductor device models for computer-aided design in power electronics"; *6th European Conference on Power Electronics*, V2, pp. 84, 1995

[15] Kang, Caiafa, Santi, Hudgins, and Palmer; "Parameter Extraction for a Power Diode Circuit Simulator Model Including Temperature Dependent Effects"; 17th *Annual Applied Power Electronics Conference and Exposition, 2002*; 10 -14 March 2002, V1, pp. 452 – 458, March 2002

[16] B. Lengeler, "Semiconductor devices suitable for use in cryogenic environments," *Cryogenics*, vol. 14, no. 8, pp. 439-447, Aug. 1974.

[17] F.J. Morin and J.P. Maita, *Phys. Rev.*, vol. 96, p. 28, 1954.

[18] F.J. Morin and J.P. Maita, *Phys. Rev.*, vol. 94, p. 1525, 1954.

[19] A. Caiafa, X. Wang, J. Hudgins, and E. Santi, "Cryogenic study and modeling of IGBTs," *IEEE PESC Rec.*, Acapulco, Mexico, June 23, 2003.